POLITECNICO DI TORINO
Repository ISTITUZIONALE

Analysis of beams with piezo-patches by node-dependent kinematic finite element method models

Original
Analysis of beams with piezo-patches by node-dependent kinematic finite element method models / Carrera, E., Zappino, E., Li, G.. - In: JOURNAL OF INTELLIGENT MATERIAL SYSTEMS AND STRUCTURES. - ISSN 1045-389X. - 29:7(2018), pp. 1379-1393. [10.1177/1045389X17733332]

Availability:
This version is available at: 11583/2706170 since: 2018-04-23T10:12:04Z

Publisher:
SAGE Publications Ltd

Published
DOI:10.1177/1045389X17733332

Terms of use:

This article is made available under terms and conditions as specified in the corresponding bibliographic description in the repository

Publisher copyright
Sage postprint/Author's Accepted Manuscript

Carrera, Erasmo; Zappino, Enrico; Li, Guohong, Analysis of beams with piezo-patches by node-dependent kinematic finite element method models, accepted for publication in JOURNAL OF INTELLIGENT MATERIAL SYSTEMS AND STRUCTURES (29 7) pp. 1379-1393. © 2018 (Copyright Holder). DOI:10.1177/1045389X17733332

(Article begins on next page)

26 October 2026

Journal of Intelligent Material Systems and Structures
XX(X):1–17
©The Author(s) 2017
Reprints and permission:
sagepub.co.uk/journalsPermissions.nav
DOI: 10.1177/ToBeAssigned
www.sagepub.com/
SAGE

Analysis of beams with piezo-patches by node-dependent kinematic FEM models

Erasmo Carrera[1], Enrico Zappino[1], and Guohong Li[1]

Abstract

This paper presents a family of one-dimensional FEM models with node-dependent kinematics for the analysis of beam structures with piezo-patches. The models proposed are built by applying Carrera Unified Formulation (CUF). CUF permits to obtain FEM stiffness matrices through so-called *fundamental nuclei* (FNs) whose form is independent of the assumptions made for the displacement/electrical field over the cross-section of a beam. In previous works, uniform kinematic assumptions have been applied to all the nodes within the same element. The present contribution proposes to use different kinematics on different nodes, leading to node-dependent kinematic FEM formulations. In such an approach, non-uniform cross-sections introduced by piezo-patches can be considered. With the help of Layer-Wise (LW) models, piezoelectric and mechanical domains each can possess individual constitutive relations. Meanwhile, node-dependent kinematics can integrate Equivalent Single Layer (ESL) models and LW models to reach an optimal balance between accuracy and use of computational resources. Static governing equations for beam elements with node-dependent kinematics accounting for electromechanical effects are derived from the Principle of Virtual Displacements (PVD). The competence of the proposed approach is validated by comparing the obtained results with solutions taken from literature and ABAQUS 3D modelling. Both extension and shear actuation mechanisms are considered.

Keywords

Beam element, Carrera Unified Formulation, Piezo-patch, Node-dependent kinematics

Introduction

Piezoelectric materials feature a reversible process that an electrical field causes straining (direct effect) while stresses cause an electric potential (reverse effect). Such an effect has prompted the development of various "smart structures". Piezoelectric components are usually bonded to the surface or embedded into the structures to act as actuators or sensors. The segmented distribution of piezoelectric patches will lead to local effects that need to be specially considered which raises the requirement for efficient modelling approaches.

An extensive variety of solutions based on either analytical methods or finite element method (FEM) have been reported. Earlier works such as the books by Tiersten (1969), Tzou and Gadre (1989), and Rogacheva (1994) presented plate and shell models accounting for the electromechanical responses of smart structures. Various 2D models have been proposed such as those based on

[1] MUL^2 group, Department of Mechanical and Aerospace Engineering, Politecnico di Torino

Corresponding author:
E. Zappino, Department of Mechanical and Aerospace Engineering Politecnico di Torino, Corso Duca degli Abruzzi 24, 10129 Torino, Italy.
Email: enrico.zappino@polito.it

This paper has been partially submitted for oral presentation at SMART2017 ECCOMAS Conference.

the Classical Lamination Theory (CLT) by Lee (1990) and Wang and Rogers (1991), First-Order Shear Deformation Theory (FSDT) models by Huang and Wu (1996) and Jonnalagadda et al. (1994), as well as Higher-Order Theory (HOT) by Mitchell and Reddy (1995). Plate element implementations were reported by researchers such as Chandrashekhara and Agarwal (1993), Batra (1995), and Suleman and Venkayya (1995). Refined 1D beam elements were developed by Robbins and Reddy (1991), Heyliger et al. (1994), Beheshti-Aval et al. (2011) to capture the interaction between the piezoelectric components and the substrate structure. Crawley and De Luis (1987) and Crawley and Anderson (1990) developed analytical models for both surface-bonded and embedded piezoelectric actuators in one-dimensional structures. Vidoli and Batra (2000) used a generalisation of the Hellinger-Prange-Reissner principle to derive constitutive relations and equilibrium equations for anisotropic 1D and 2D models for piezoelectric bodies. A zig-zag theory for laminated plates was extended to the electromechanical case for the analysis of beams and plates with piezoelectric components by Kapuria (2001, 2004). Brick elements were used by Batra and Liang (1997) and Hauch (1995). It has been widely recognised that solid elements are comparatively computational costly and less efficient when applied to model thin piezoelectric components. More detailed reviews of analysis and modelling methods for laminates with piezoelectric components can be found in Saravanos and Heyliger (1999); Benjeddou (2000); Wang and Yang (2000); Mackerle (2003); Kapuria et al. (2010).

Carrera (2002) proposed Unified Formulation (CUF) as a new methodology to construct refined 1D and 2D models. CUF introduces thickness functions $F_\tau(z)$ to 2D theories and $F_\tau(x,z)$ to 1D models. These functions refine the displacement field in the through-the-thickness domain of 2D models and over the cross-section of 1D models, which can employ either series expansions or interpolation polynomials. In the framework of CUF, various theories based on both Equivalent Single Layer (ESL) and Layer-wise (LW) models can be depicted as reported by Cinefra et al. (2015b) and Cinefra and Valvano (2016). The introduction of *fundamental nuclei* (FNs) allows the governing equations to be derived in a compact manner as explicated by Carrera et al. (2016, 2017). Based on CUF, Carrera and Fagiano (2007), Carrera et al. (2010), and Carrera and Robaldo (2010) proposed advanced plate elements with *a priori* continuous transverse electromechanical variables by applying Reissner Mixed Variational Theorem (RMVT). The application of the CUF to piezo-electric beams was presented by Koutsawa et al. (2015, 2013) and Biscani et al. (2011) used the Arelquin approach to couple piezo-beams with different kinematics assumptions. Cinefra et al. (2015a) adopted an axiomatic/asymptotic technique to detect the "best" plate model to capture the static response of piezoelectric plates, in which the models are constructed by employing the Principle of Virtual Displacements (PVD). Miglioretti et al. (2014) and Zappino et al. (2016) adopted refined electromechanical beam FEM models with variable kinematics in the analysis of structures with piezoelectric components, which are based on PVD. More systematic discussions and a variety of refined CUF-based models for the analysis of smart structures can be found in Carrera et al. (2011a).

Notably, CUF makes it possible to define "nodal kinematics", which means that the kinematic assumptions can be further related to specific FEM nodes, leading to node-dependent kinematic FEM models. For CUF-based plate models, this suggests that the thickness functions $F_\tau(z)$ can be individually defined on different nodes; for refined beam elements, this method enables each node to possess independent cross-section functions $F_\tau(x,z)$. Node-dependent kinematics based on CUF, as an innovative methodology to construct advanced FEM models, was firstly suggested by Carrera and Zappino (2014, 2017). Except for providing the convenience to implement global-local models as has been demonstrated by Zappino et al. (2017), an alternative application of such an approach is to construct FEM models for the analysis of structures with embedded or surface-mounted piezoelectric components, wherein different constitutive relations can be separately applied to the substrate structure and the piezoelectric components. In the present work, based on node-dependent kinematics, an approach to constructing advanced one-dimensional FEM models for the analysis of structures with piezo-patches is presented. Models with variable

LW/ESL capabilities from node to node are implemented. The competence of the proposed approach is demonstrated with cantilever beam structures with either surface-mounted or embedded piezo-patches. Both extension and shear actuation mechanisms are taken into account.

Refined one-dimensional electromechanical model

Preliminaries

Considering the coupling between electric and mechanical field, by treating the electric potential ϕ as a primary variable, a generalised displacement vector $\boldsymbol{q}$ can be adopted:

$$\boldsymbol{q} = \{u_x, u_y, u_z, \phi\}^T \tag{1}$$

and the electric field vector $\boldsymbol{E}$ can be derived as:

$$\boldsymbol{E} = \{E_x, E_y, E_z\}^T = \{\partial_x, \partial_y, \partial_z\}^T \phi \tag{2}$$

The generalised strain vector, $\bar{\varepsilon}$, can be written as:

$$\bar{\boldsymbol{\varepsilon}} = \{\varepsilon_{xx}, \varepsilon_{yy}, \varepsilon_{zz}, \varepsilon_{xz}, \varepsilon_{yz}, \varepsilon_{xy}, E_x, E_y, E_z\}^T = \boldsymbol{D}\boldsymbol{q} \tag{3}$$

where the matrix of the differential operator $\boldsymbol{D}$ is:

$$\boldsymbol{D} = \begin{bmatrix} \frac{\partial}{\partial x} & 0 & 0 & 0 \\ 0 & \frac{\partial}{\partial y} & 0 & 0 \\ 0 & 0 & \frac{\partial}{\partial z} & 0 \\ \frac{\partial}{\partial z} & 0 & \frac{\partial}{\partial x} & 0 \\ 0 & \frac{\partial}{\partial z} & \frac{\partial}{\partial y} & 0 \\ \frac{\partial}{\partial y} & \frac{\partial}{\partial x} & 0 & 0 \\ 0 & 0 & 0 & \frac{\partial}{\partial x} \\ 0 & 0 & 0 & \frac{\partial}{\partial y} \\ 0 & 0 & 0 & \frac{\partial}{\partial z} \end{bmatrix} \tag{4}$$

The electromechanical constitutive equations (*e-form*) in the case of the principle of virtual displacement (PVD) can be expressed as follows:

$$\begin{aligned} \boldsymbol{\sigma} &= \tilde{\boldsymbol{C}}\boldsymbol{\varepsilon} - \tilde{\boldsymbol{e}}^T \boldsymbol{E} \\ \boldsymbol{D}_e &= \tilde{\boldsymbol{e}}\boldsymbol{\varepsilon} + \tilde{\boldsymbol{\chi}}^T \boldsymbol{E} \end{aligned} \tag{5}$$

in which $\boldsymbol{D}_e$ is the electric displacement vector $\{D_x, D_y, D_z\}^T$, and $\boldsymbol{\sigma}$ is the mechanical stress vector, $\boldsymbol{C}$ the matrix of mechanical material coefficients. Considering a rotation θ with respect to z axis, the dielectric permittivity matrix $\boldsymbol{\chi}$ will appear like:

$$\boldsymbol{\chi} = \begin{bmatrix} \tilde{\chi}_{11} & \tilde{\chi}_{12} & 0 \\ \tilde{\chi}_{21} & \tilde{\chi}_{22} & 0 \\ 0 & 0 & \tilde{\chi}_{33} \end{bmatrix} \tag{6}$$

meanwhile, the piezoelectric stiffness coefficient matrix $\boldsymbol{e}$ will be as follows:

$$\boldsymbol{e} = \begin{bmatrix} \tilde{e}_{11} & \tilde{e}_{12} & \tilde{e}_{13} & \tilde{e}_{14} & \tilde{e}_{15} & \tilde{e}_{16} \\ \tilde{e}_{21} & \tilde{e}_{22} & \tilde{e}_{23} & \tilde{e}_{24} & \tilde{e}_{25} & \tilde{e}_{26} \\ \tilde{e}_{31} & \tilde{e}_{32} & \tilde{e}_{33} & \tilde{e}_{34} & \tilde{e}_{35} & \tilde{e}_{36} \end{bmatrix} \tag{7}$$

The generalized stress vector can be arranged as:

$$\bar{\boldsymbol{\sigma}} = \{\sigma_{xx}, \sigma_{yy}, \sigma_{zz}, \sigma_{xz}, \sigma_{yz}, \sigma_{xy}, D_x, D_y, D_z\}^T \tag{8}$$

The generalised stress vector can be written as in Equation 9, which in a more compact form can be expressed as:

$$\bar{\boldsymbol{\sigma}} = \tilde{\boldsymbol{H}}\bar{\boldsymbol{\varepsilon}} \tag{10}$$

If the piezoelectric components are poled in the third material axis, the dielectric permittivity matrix $\boldsymbol{\chi}$ is:

$$\boldsymbol{\chi} = \begin{bmatrix} \chi_{11} & 0 & 0 \\ 0 & \chi_{22} & 0 \\ 0 & 0 & \chi_{33} \end{bmatrix} \tag{11}$$

and the piezoelectric stiffness coefficient matrix $\boldsymbol{e}$ would be in the form of the following expression:

$$\boldsymbol{e} = \begin{bmatrix} 0 & 0 & 0 & e_{15} & 0 & 0 \\ 0 & 0 & 0 & 0 & e_{24} & 0 \\ e_{31} & e_{32} & e_{33} & 0 & 0 & 0 \end{bmatrix} \tag{12}$$

which after a rotation around z will become:

$$\tilde{\boldsymbol{e}} = \begin{bmatrix} 0 & 0 & 0 & \tilde{e}_{14} & \tilde{e}_{15} & 0 \\ 0 & 0 & 0 & \tilde{e}_{24} & \tilde{e}_{25} & 0 \\ \tilde{e}_{31} & \tilde{e}_{32} & \tilde{e}_{33} & 0 & 0 & \tilde{e}_{36} \end{bmatrix} \tag{13}$$

$$\begin{Bmatrix} \sigma_{xx} \\ \sigma_{yy} \\ \sigma_{zz} \\ \sigma_{xz} \\ \sigma_{yz} \\ \sigma_{xy} \\ D_x \\ D_y \\ D_z \end{Bmatrix} = \begin{bmatrix} \tilde{C}_{11} & \tilde{C}_{12} & \tilde{C}_{13} & 0 & 0 & \tilde{C}_{16} & -\tilde{e}_{11} & -\tilde{e}_{21} & -\tilde{e}_{31} \\ \tilde{C}_{21} & \tilde{C}_{22} & \tilde{C}_{23} & 0 & 0 & \tilde{C}_{26} & -\tilde{e}_{12} & -\tilde{e}_{22} & -\tilde{e}_{32} \\ \tilde{C}_{31} & \tilde{C}_{32} & \tilde{C}_{33} & 0 & 0 & \tilde{C}_{36} & -\tilde{e}_{13} & -\tilde{e}_{23} & -\tilde{e}_{33} \\ 0 & 0 & 0 & \tilde{C}_{44} & \tilde{C}_{45} & 0 & -\tilde{e}_{14} & -\tilde{e}_{24} & -\tilde{e}_{34} \\ 0 & 0 & 0 & \tilde{C}_{54} & \tilde{C}_{55} & 0 & -\tilde{e}_{15} & -\tilde{e}_{25} & -\tilde{e}_{35} \\ \tilde{C}_{61} & \tilde{C}_{62} & \tilde{C}_{63} & 0 & 0 & \tilde{C}_{66} & -\tilde{e}_{16} & -\tilde{e}_{26} & -\tilde{e}_{36} \\ \tilde{e}_{11} & \tilde{e}_{12} & \tilde{e}_{13} & \tilde{e}_{14} & \tilde{e}_{15} & \tilde{e}_{16} & \tilde{\chi}_{11} & \tilde{\chi}_{12} & 0 \\ \tilde{e}_{21} & \tilde{e}_{22} & \tilde{e}_{23} & \tilde{e}_{24} & \tilde{e}_{25} & \tilde{e}_{26} & \tilde{\chi}_{21} & \tilde{\chi}_{22} & 0 \\ \tilde{e}_{31} & \tilde{e}_{32} & \tilde{e}_{33} & \tilde{e}_{34} & \tilde{e}_{35} & \tilde{e}_{36} & 0 & 0 & \tilde{\chi}_{33} \end{bmatrix} \begin{Bmatrix} \varepsilon_{xx} \\ \varepsilon_{yy} \\ \varepsilon_{zz} \\ \varepsilon_{xz} \\ \varepsilon_{yz} \\ \varepsilon_{xy} \\ E_x \\ E_y \\ E_z \end{Bmatrix} \tag{9}$$

elsewise, if the polarization direction is along the second axis of the material coordinate system, the dielectric permittivity $\boldsymbol{\chi}$ and piezoelectric stiffness matrix $\boldsymbol{e}$ would read:

$$\boldsymbol{\chi} = \begin{bmatrix} \chi_{22} & 0 & 0 \\ 0 & \chi_{33} & 0 \\ 0 & 0 & \chi_{11} \end{bmatrix} \tag{14}$$

$$\boldsymbol{e} = \begin{bmatrix} 0 & 0 & 0 & 0 & 0 & e_{24} \\ e_{32} & e_{33} & e_{31} & 0 & 0 & 0 \\ 0 & 0 & 0 & 0 & e_{15} & 0 \end{bmatrix} \tag{15}$$

accordingly when rotated in z the $\boldsymbol{e}$ will become:

$$\tilde{\boldsymbol{e}} = \begin{bmatrix} \tilde{e}_{11} & \tilde{e}_{12} & \tilde{e}_{13} & 0 & 0 & \tilde{e}_{16} \\ \tilde{e}_{21} & \tilde{e}_{22} & \tilde{e}_{23} & 0 & 0 & \tilde{e}_{26} \\ 0 & 0 & 0 & \tilde{e}_{34} & \tilde{e}_{35} & 0 \end{bmatrix} \tag{16}$$

For more details about the rotation of piezoelectric material coefficient matrices the reader is referred to Kpeky et al. (2017); Benjeddou et al. (1997); Kapuria and Hagedorn (2007).

CUF-based beam elements with node-dependent kinematics

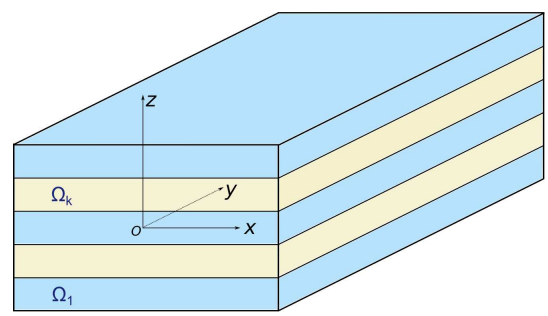

Figure 1. Geometry and reference system of a laminated beam model

This section presents the refined one-dimensional models for electromechanical analysis. For a slender layered structure, the reference coordinate system is as shown in Figure 1. According to CUF, beam models can be refined by further expanding a generic function $F_\tau(x,z)$ defined on the cross-section, leading to the following expression:

$$\boldsymbol{u} = F_\tau(x,z)\boldsymbol{u}_\tau(y) \qquad \tau = 1, \cdots, M. \tag{17}$$

in which M represents the number of expansion terms. $\boldsymbol{u} = \{u, v, w\}^T$ is the mechanical displacement vector, and $\boldsymbol{u}_\tau(y)$ is a vector defined along the axis of the beam. By extending Equation 17 into the electromechanical case, one can obtain:

$$\boldsymbol{q} = F_\tau(x,z)\boldsymbol{q}_\tau(y) \qquad \tau = 1, \cdots, M. \tag{18}$$

where $\boldsymbol{q} = \{u, v, w, \phi\}^T$ is the generalized electromechanical displacement vector. To define the cross-section functions $F_\tau(x,z)$, various theories can be employed. In the analysis of multi-layered structures, Taylor-like expansions

apply to ESL models, and Lagrange-type expansions suit the LW framework.

Nodal kinematics with Taylor Expansions (TE)

The TE-type kinematics adopts Taylor series to build the cross-section functions $F_\tau(x,z)$, in which the series are taken as $x^m z^n$ (where m and n are positive integers). As an example, the displacement field based on the second-order TE expansions can be expressed as:

$$\begin{cases} u = F_1u_1 + F_2u_2 + F_3u_3 + F_4u_4 + F_5u_5 + F_6u_6 \\ v = F_1v_1 + F_2v_2 + F_3v_3 + F_4v_4 + F_5v_5 + F_6v_6 \\ w = F_1w_1 + F_2w_2 + F_3w_3 + F_4w_4 + F_5w_5 + F_6w_6 \\ \phi = F_1\phi_1 + F_2\phi_2 + F_3\phi_3 + F_4\phi_4 + F_5\phi_5 + F_6\phi_6 \end{cases} \tag{19}$$

where the terms of F_τ read as follows:

$$\begin{gathered} F_1 = 1, \\ F_2 = x, \quad F_3 = z, \\ F_4 = x^2, \quad F_5 = xz, \quad F_6 = z^2. \end{gathered} \tag{20}$$

Kinematics based on Taylor series can be denoted as "TEn", where n indicates the highest order of the polynomials adopted. Timoshenko beam theory can be treated as a particular case of a TE model. Euler-Bernoulli beam model can be implemented in FEM models by enforcing a significant penalty to the corresponding components of the stiffness matrix to eliminate the degrees of freedom not present in the model.

Nodal kinematics with Lagrange Expansions (LE)

Lagrange interpolation polynomials can also be applied to construct the cross-section functions, leading to LE-type kinematics. Taking the Lagrange interpolation polynomials on the four tip points of a rectangular (LE4) as an example, the expansion terms are:

$$F_\tau = \frac{1}{4}(1 + rr_\tau)(1 + ss_\tau) \qquad \tau = 1,2,3,4 \tag{21}$$

where r and s are the coordinates in the parametric reference system of a quadrilateral domain and vary from -1 to 1. Similarly, two-parameter Lagrange interpolation polynomials over nine points will lead to expansions denoted as "LE9", and their explicit expressions are:

$$\begin{aligned} F_\tau &= \frac{1}{4}(r^2 + rr_\tau)(s^2 + ss_\tau) && \tau = 1,3,5,7 \\ F_\tau &= \frac{1}{2}s_\tau^2(s^2 + ss_\tau)(1 - r^2) + \frac{1}{2}r_\tau^2(r^2 + rr_\tau)(1 - s^2) \\ & && \tau = 2,4,6,8 \\ F_\tau &= (1 - r^2)(1 - s^2) && \tau = 9 \end{aligned} \tag{22}$$

When displacement-based LE models are employed, the degrees of freedom of the FEM models are the physical translational displacements of the cross-sectional nodes (interpolation points). By using LE expansions, the continuity of transverse shear stresses at layer interfaces can be naturally captured, and the zig-zag distribution of shear deformation can be adequately approximated. In Carrera et al. (2011b) and Carrera et al. (2014) more detailed discussions are given.

CUF-based beam element with node-dependent kinematics

When CUF-based cross-section functions are applied to formulate beam elements, Lagrangian shape functions $N_i(y)$ can be used to approximate the axial unknown vector $\boldsymbol{q}_\tau(y)$:

$$\boldsymbol{q} = N_i(y)F_\tau(x,z)\boldsymbol{q}_{i\tau}(y) \quad \tau = 1,\cdots,M; i = 1,\cdots,N_n. \tag{23}$$

If F_τ depend on specific nodes, a beam element with node-dependent kinematics can be constructed, whose displacement functions can be described as:

$$\boldsymbol{q} = N_i(y)F_\tau^i(x,z)\boldsymbol{q}_{i\tau}(y) \quad \tau = 1,\cdots,M; i = 1,\cdots,N_n. \tag{24}$$

With the help of the Lagrangian shape functions, individually defined nodal kinematics can be interpolated over the axial domain of a beam element, obtaining

elements with variable LW/ESL capabilities from node to node. Figure 2 illustrates a beam element with four nodes formulated with node-dependent kinematics, in which on node 1 and node 2 TE kinematics are used, while node 3 and node 4 employ LE-type cross-section functions. F_τ^3 possesses nine expansion terms defined on the whole cross-section domain, and F_τ^4 includes 16 terms belong to nine sub-domains on the cross-section and their assembly follows the LW framework. Separately defined nodal-kinematics can be further interpolated over the axial domain by the shape functions $N_i(y)$ to form a beam element. In such a way, a "kinematic variation" can be realised which can naturally guarantee the continuity of displacement field.

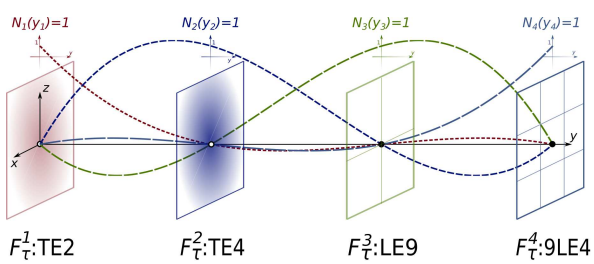

Figure 2. A B4 element with node-dependent kinematics

Electromechanical governing equation of node-dependent kinematic beam elements

The stiffness of the beam elements, as well as the external load vector, can be derived by applying the principle of virtual displacement (PVD). By substituting the constitutive equations, the following expression can be attained:

$$\delta L_{int} = \int_V \delta\bar{\boldsymbol{\varepsilon}}^T \bar{\boldsymbol{\sigma}} dV = \delta L_{ext} \tag{25}$$

If the geometrical relations and shape functions are substituted into the above expression, one can obtain:

$$\delta L_{int} = \delta \boldsymbol{q}_{sj} \int_V N_j \boldsymbol{I} F_s^j \boldsymbol{D}^T \tilde{\boldsymbol{H}} \boldsymbol{D} F_\tau^i \boldsymbol{I} N_i dV \boldsymbol{q}_{i\tau} \tag{26}$$

in which $\boldsymbol{I}$ is a 4×4 identity matrix. In a more compact form, the above expression can be written as:

$$\delta L_{int} = \delta \boldsymbol{q}_{sj}^T \boldsymbol{K}_{ij\tau s} \boldsymbol{q}_{\tau i} \tag{27}$$

where $\boldsymbol{K}_{ij\tau s}$ is the stiffness matrix, which contains the *fundamental nuclei* (FNs), and it can be expressed as:

$$\boldsymbol{K}_{ij\tau s} = \int_V N_j \boldsymbol{I} F_s^j \boldsymbol{D}^T \tilde{\boldsymbol{H}} \boldsymbol{D} F_\tau^i \boldsymbol{I} N_i dV \tag{28}$$

The virtual work due to the load $\boldsymbol{P} = \{P_x, P_y, P_z, P_\phi\}$ can be expressed as:

$$\delta L_{ext} = \int_V \delta \boldsymbol{q}^T \boldsymbol{P} dV \tag{29}$$

Considering the displacement function Equation 24, the external work can be written as:

$$\delta L_{ext} = \delta \boldsymbol{q}_{sj}^T \int_V F_s^j N_j \boldsymbol{P} dV = \delta \boldsymbol{q}_{sj}^T \cdot \boldsymbol{p}_{sj} \tag{30}$$

where $\boldsymbol{p}_{sj}$ is the expression of the load vector for FEM. Then the governing equation for a static problem can be expresses as:

$$\delta \boldsymbol{q}_{sj} : \quad \boldsymbol{K}_{ij\tau s} \cdot \boldsymbol{q}_{\tau i} = \boldsymbol{p}_{sj} \tag{31}$$

Modelling of piezo-patches with node-dependent kinematics

The modelling of the piezo-patches with CUF-based node-dependent kinematics is illustrated in Figure 3. The same approach also applies to embedded piezo-patches. In this example, the piezo-patch is bonded on the top surface of the elastic base, as shown in Figure 3 (a). The whole slender structure is divided into three B2 beam elements, elements *A*, *B* and *C*. Four nodes (*a*,*b*,*c*,*d*) are used to build the FE model. The present node-dependent kinematics approach has been used to impose a layer-wise model in the nodes of the element where the piezo-patch is placed and a lower-order model, based on the TE-type kinematic, in the other parts of the structure as illustrated in Figure 3 (b). In particular the LW model based on a LE-type kinematic has been used at node *b* and *c* while the TE-type kinematic has been used at nodes *a* and *d*.

Figure 3 (c) illustrates the assembly procedure of stiffness matrix for the above described FEM model. $\boldsymbol{K}_{ab}^1/\boldsymbol{K}_{ba}^1$, $\boldsymbol{K}_{bc}^1/\boldsymbol{K}_{cb}^1$, and $\boldsymbol{K}_{cd}^1/\boldsymbol{K}_{dc}^1$ represent the coupling between the nodes within the pure mechanical domain;

$\boldsymbol{K}^2_{bc}$ and $\boldsymbol{K}^2_{cb}$ indicate the coupling between the nodes lie in the piezoelectric region. It is worth noting that the coupling stiffness matrices between nodes in the same element will mostly become rectangular; in generally used FEM models with uniform kinematic assumptions, they are square matrices. Since the cross-sectional nodes belonging to the piezoelectric zone each has an extra degree of freedom for electrical potential except for the mechanical ones, the FNs of electromechanical stiffness are 4×4 rather than 3×3. Specially, on the cross-sectional nodes located at the interfaces of the piezoelectric patch and the elastic base, to each four degrees of freedom are assigned, but in the integration to obtain the stiffness of the base structure only the mechanical ones will be considered. It should be pointed out that the interpolation through the shape functions $N_i(y)$ exists only among the variables within the domain with the same constitutive relations. With node-dependent kinematic beam models, in such a way the abrupt change of the cross-section feature along the axis because of the piezo-patches can be properly . The introduction of variable ESL(TE)/LW(LE) capabilities is expected to reduce the total degrees of freedom of the FEM models.

Numerical results

Cantilever beams with piezo-patches considering extension and shear mechanisms

In this section, two types of cantilever beams are considered, which are illustrated in Figure 4: configuration (a) for extension actuation mechanism (EAM), and configuration (b) for shear actuation mechanism (SAM). In both of the two configurations, the piezoelectrical components occupy the entire width range (in x direction). Such benchmark cases have been studied by various researchers such as Sun and Zhang (1995); Zhang and Sun (1996) and Benjeddou et al. (1997), as well as Kpeky et al. (2017).

The piezoelectric components are poled in the thickness direction (z) for the extension case, and axial direction (which is y in the present work) for the shear actuation case. To actuate the beam, different electrical potentials values (voltage) are applied on the top and bottom surface of the piezo-patches: voltage differences $\Delta\phi = \phi_{bottom} - \phi_{top} = 10$V for the upper patch and $\Delta\phi = -10$V for the lower one are used respectively in the extension configuration; $\Delta\phi = 20$V is used for the shear mechanism. The piezoelectric components are made of PZT-5H, whose material coefficients have been listed in Table 1, and the substrate structures employ aluminum which has the Young's modulus $E = 70.3$GPa and Poisson's ratio $\nu = 0.345$. The width of the beams is $a = 0.02$m, and the length is $b = 0.1$m. In the extension configuration, the patches have equal thickness $h_p = 0.001$m, and the maximum thickness is $h_e = 0.018$m; while the single patch in the shear situation is as thick as 0.002m, and the total thickness is $h_s = 0.018$m. In both of the two configurations, the total thickness of the aluminum substrate is $h = 0.016$m. Two cases are considered:

- *Case A*: the piezo-patches cover the whole length range;
- *Case B*: the piezoelectric components have the length $c = 0.01$m and variable positions along the axial direction from $d = 0.01$m to $d = 0.09$m.

For the shear mechanism situation in *Case B*, the rest part of the core except the piezo-patch uses a foam material with $E = 35.3$MPa and $\nu = 0.38$.

Numerical results for *Case A* are obtained with uniform LE nodal kinematics denoted as "12LE9", which discretizes the cross-section into 12 sub-domains, as illustrated in Figure 5. Note that when Lagrange expansions are adopted to describe the kinematics on a cross-section of a beam, each expansion term possesses specific physical coordinates. Along the longitudinal direction, the structure is divided into 20 beam elements, each has 4 FEM nodes. The obtained results are compared with the solutions provided by Benjeddou et al. (1997) and Kpeky et al. (2017) as well as those given by ABAQUS 3D modelling. The ABAQUS models employ eight layers of C3D20R mechanical brick elements and another eight layers of C3D20RE piezoelectric brick elements, uniformly 8×40 ($x \times y$) in each layer. The results given by Benjeddou et al. (1997) were obtained through a beam element model in which the displacement assumptions were layer-wisely

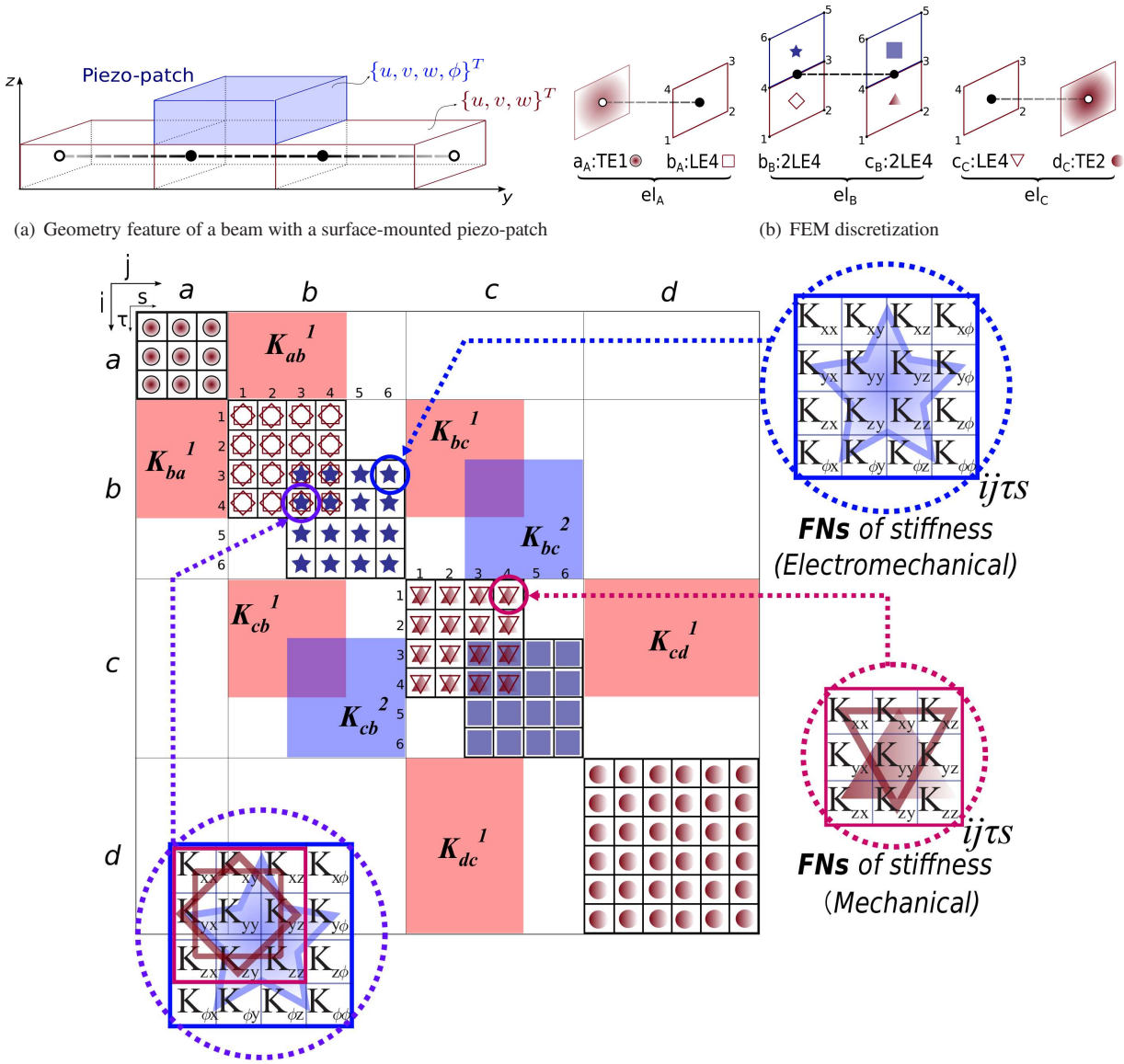

(a) Geometry feature of a beam with a surface-mounted piezo-patch

(b) FEM discretization

(c) Assembly of structural stiffness matrix

Figure 3. Stiffness matrix assembly of a beam model with a piezo-patch

Table 1. Material properties of PZT-5H

C_{11},C_{22},C_{33} [GPa]	C_{12} [GPa]	C_{13},C_{23} [GPa]	C_{44},C_{55},C_{66} [GPa]	e_{15},e_{24} [C/m^2]	e_{31},e_{32} [C/m^2]	e_{33} [C/m^2]	χ_{11},χ_{22} [F/m]	χ_{33} [F/m]
126	79.5	84.1	23.0	17.0	-6.5	23.3	1.503×10^{-8}	1.30×10^{-8}

defined (more specifically the faces employed Bernoulli-Euler theory while the cores adopted Timoshenko theory), and the displacement continuity was enforced at layer interfaces. Kpeky et al. (2017) reached their solution through solid-shell piezoelectric elements SHB8PSE and SHB20E.

The variation of deflection along the beam axis at the cross-sectional central point (lines A) and at one of the

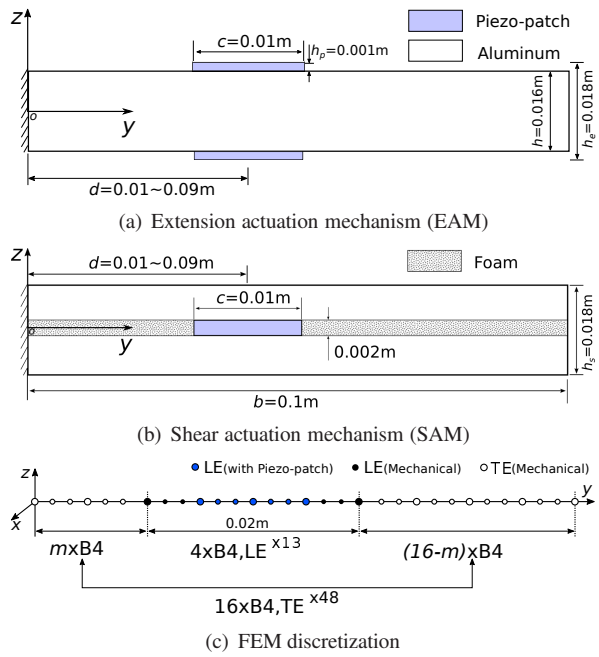

(a) Extension actuation mechanism (EAM)

(b) Shear actuation mechanism (SAM)

(c) FEM discretization

Figure 4. Geometrical feature and FEM discretization of slender beams with piezo-patches

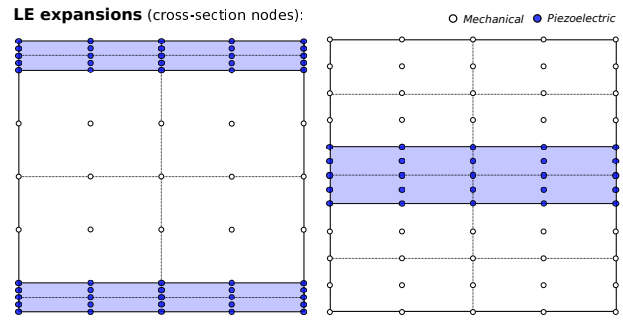

(a) EAM

(b) SAM

Figure 5. 12LE9: discretization of cross-sections with LE, piezo-patches cover entire length of the beams (*Case A*)

upper corners (lines B) for the two configurations in *Case A* are shown in Figure 6. Table 2 compares the deflection on two sets of locations on the free-end cross-sections for both EAM and SAM configurations. It should be noted that in the reference literature, locations on the cross-section where the deflections were reported was not explicitly given. It can be observed that the current solutions agree well with the ABAQUS results. For the EAM in *Case A*, the present solutions for deflection are comparatively low than those presented by Benjeddou et al. (1997), which were obtained by applying plane-stress constitutive relations. Meanwhile, the deflection on Line B $(a/2, y, h_e/2)$ matches the distribution proposed by Kpeky et al. (2017). For the shear configuration in *Case A*, the current solution shows good agreement with those by Benjeddou et al. (1997) as well as Kpeky et al. (2017).

Table 2. Deflection evaluation on the free-end cross-section of the beams in *Case A*

	$w[10^{-7}\text{m}]$			
	EAM		SAM	
	$(0, b, 0)$	$(\frac{a}{2}, b, \frac{h_e}{2})$	$(0, b, 0)$	$(\frac{a}{2}, b, \frac{h_s}{2})$
ABAQUS	3.749	3.913	1.184	1.184
12LE9	3.748	3.897	1.184	1.184

The models with the same uniform 12LE9 sectional kinematics are also applied to reach the numerical solutions to *Case B*, and the results are as shown in Figure 7. Note here the 12LE9 refers to the model adopted in the region with the piezo-patches. It can be observed that the results based on 12LE9 are in good agreement with the reference solutions taken from literature Kpeky et al. (2017). The results presented by Kpeky et al. (2017) which achieved by considering three-dimensional constitutive relations. For the extension configuration in *Case B*, when the piezo-patches are located near the free end (from around $d = 0.07$m to $d = 0.09$m), theoretically the actuator efficiency will decrease, which means the deflection at the free end will drop rather than increase, as the curve for Point a$(0, b, 0)$ shown in Figure 7(a). Meanwhile, for the extension configuration in *Case B*, with the increase of d, the maximum deflection will move from the vertexes ofthe base structure to the corner points of the patch (Points b), as shown in Figure 7. This may explain the up-going trend at the end of the curve given in Kpeky et al. (2017). Different from the extension case, for the shear mechanism, the variation of the free end deflection with d shows an obvious non-linear trend. The actuator efficiency increases slowly when the piezo-patch moves away from the clamped end then drops quickly after peaking at around $d = 0.02$m. It can be noticed that the curve corresponds to point d $(a/2, b, h_s/2)$ matches the solution of Kpeky et al. (2017) very well.

To reduce the computational costs, FEM models with variable ESL/LW kinematics from node to node are

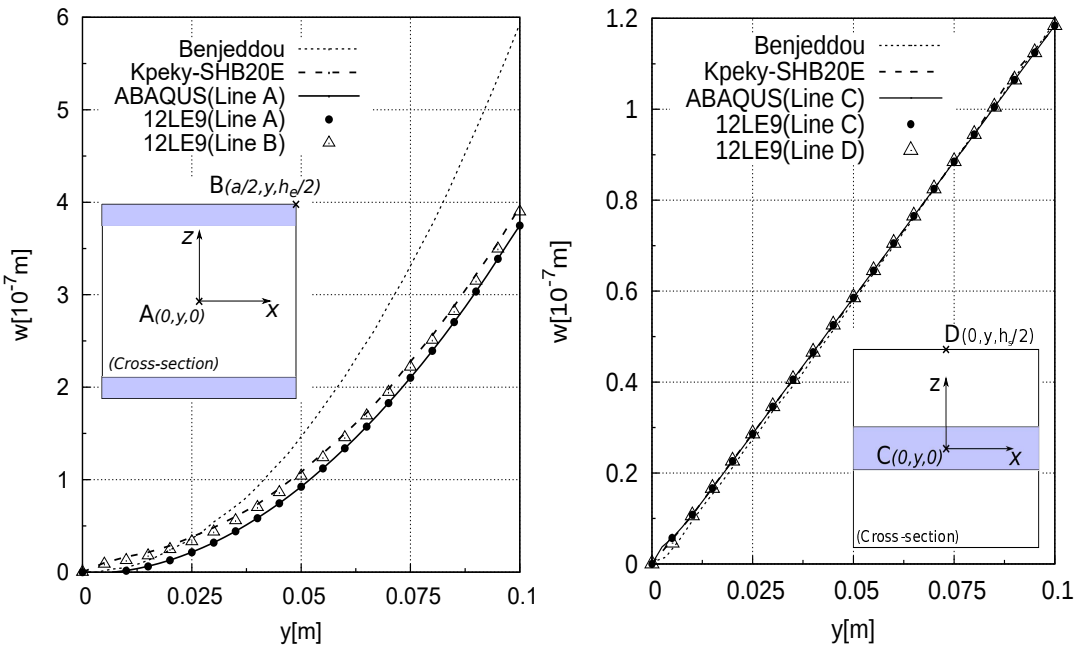

(a) EAM (b) SAM

Figure 6. Distribution of w along the axis of the beam, piezo-patches cover the entire length (*Case A*)

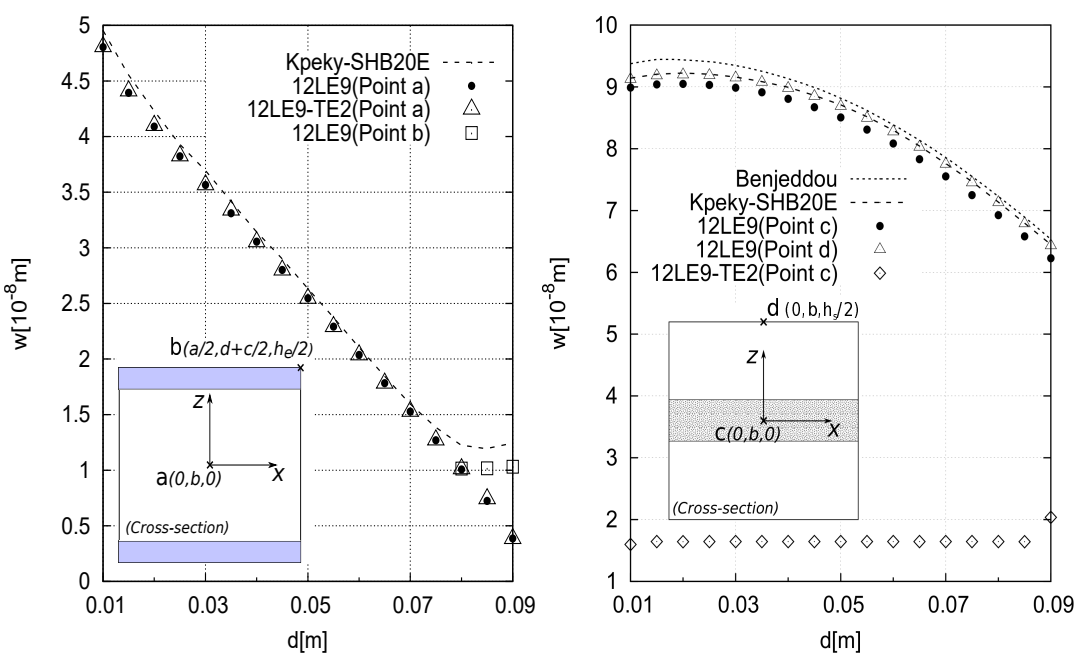

(a) EAM (b) SAM

Figure 7. Deflection on the free end of the cantilever beams with piezo-patches in *Case B*

adopted in the analysis for the configurations in *Case B*. The corresponding assignment of nodal kinematics is illustrated in Figure 4. In a region which is as long as $2c = 0.02$m containing the piezo-patches discretized into four B4 elements, nodal kinematics 12LE9 is applied to the corresponding nodes; the rest of the beam (with 16

B4 elements) is modelled with nodal kinematics adopting TE. When Taylor series to the second order are used in combination with 12LE9, the model can be denoted as "12LE9-TE2" . The obtained numerical results have been compared with those achieved with uniform 12LE9 kinematics in Figure 5. For the extension configuration in *Case B*, FEM model 12LE9-TE2 leads to the solution in high agreement with mono-kinematic model 12LE9, while reducing the total degrees of freedom by 42.5% (from 5765 to 3317), as summarised in Table 3.

Table 3. Deflection at the center of the free end of the beam for EAM in *Case B*

d[m]	$w^*[10^{-8}\text{m}]$	
	12LE9	12LE9-TE2
0.01	4.805	4.805
0.03	3.565	3.563
0.05	2.546	2.543
0.07	1.527	1.527
0.09	0.3863	0.3826
DOFs	5765	3317

$*$At Point a$(0, b, 0)$

Whereas, in Figure 7 it can be observed that the model 12LE9-TE2 fails to give reasonable response for the shear configurations in *Case B*. This is caused by the intrinsic drawback of cross-section functions based on Taylor expansions in capturing transverse shearing effects in laminated structures. Such a disadvantage makes the model 12LE9-TE2 not able to transfer the shear actuation with satisfactory accuracy. Taking the results of the shear configuration with $d = 0.01$m (whose clamped end is modelled with LE) as an example, the deflection along the axis shown in Figure 8 obtained with model 12LE9-TE2 remains constant in the region on the free-end side where TE kinematics is adopted. Through-the-thickness variation of transverse shear strain ε_{yz} and stress σ_{yz} on the mid-span ($y = b/2$) cross-section are shown in Figure 9. It can be noticed that TE kinematics leads to continuous transverse strain but discontinuous transverse stress variation, which means that the shear actuation from the piezo-patch is not transferred properly. Comparatively, Lagrange expansions have good performance when applied to the shear mechanism situation. Note that in the extension case the bending response of the beam is caused by the in-plane normal straining of the beam. For more detailed discussion on TE kinematics in capturing transverse shear effects in laminated structures, the reader is referred to Carrera (1996) and Carrera et al. (2013).

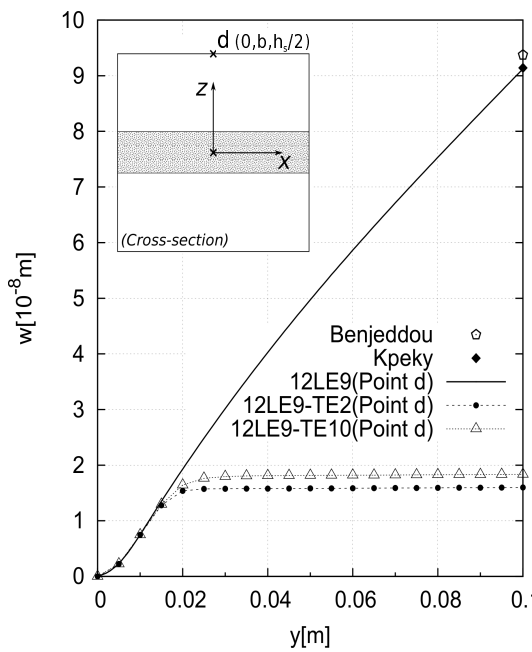

Figure 8. Deflection at the free-end center on the SAM configuration with $d = 0.01$m in *Case B*

A cantilever beam with one surface-mounted piezo-patch

A slender aluminum beam actuated by a PZT piezoelectric patch is considered in this section as a numerical assessment case, of which the reference solution is provided by Biscani et al. (2012). The geometry feature of the structure is shown in Figure 10, which has width $a = 0.01$m and length $b = 0.1$m. The thickness of the aluminum beam and the piezo-patch are $h = 0.002$m and $h_p = 0.001$m, respectively. The square piezo-patch made of PZT-4 (refer to Table 4 for the material properties) is bonded to the top surface of the aluminum beam in the vicinity of the clamped end, which takes up the whole width range. In this assessment case, the piezo-patch acts as an actuator, and an electrical potential of 1V is defined on its top surface and 0V on the bottom.

The FEM discretization scheme of the structure has been illustrated in Figure 10. The slender structure is divided

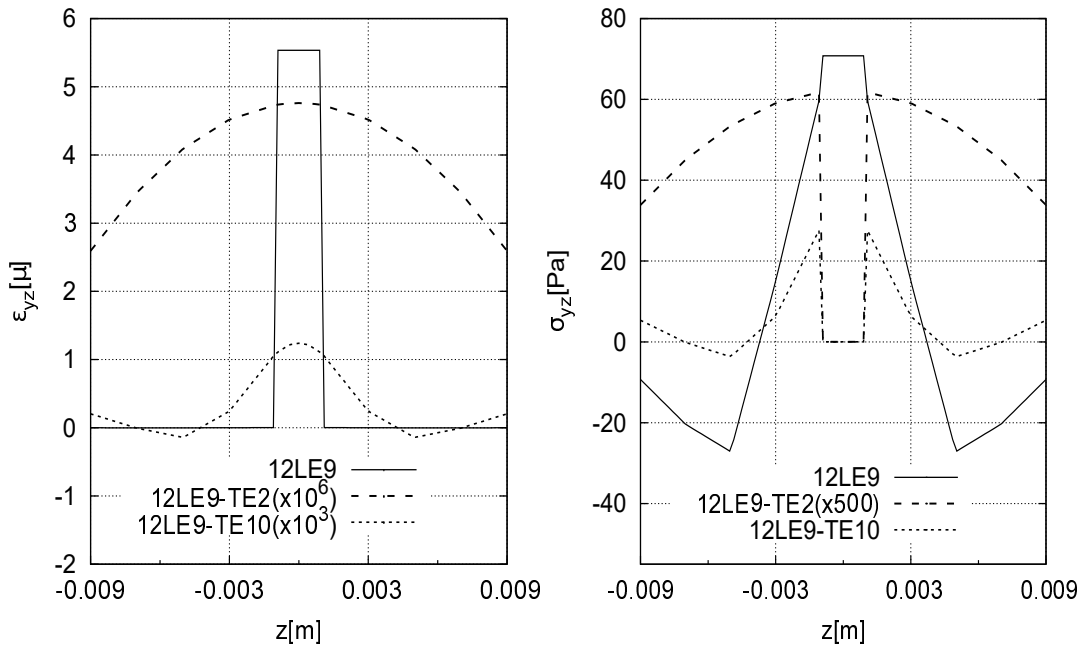

(a) $\varepsilon_{yz}, (0, b/2, z)$ (b) $\sigma_{yz}, (0, b/2, z)$

Figure 9. Deflection and stress evaluation on the SAM configuration with $d = 0.01$m in *Case B*

into three zones along the axial direction y, and in the zones containing and neighbouring the piezo-patch, $2 \times m$ uniformly distributed B4 elements are assigned, while in the rest 80% of the structure another m B4 elements are employed. Thus in total $3 \times m$ refined B4 elements will be adopted to capture the structural response. For brevity, different FEM models are denoted by the nodal kinematics defined on the cross-sections that contain the piezo-patch, in which the piezoelectric and mechanical domain employ the same kinematics. For example, 4LE9 refers to a model uses 2LE9 in the piezoelectric cross-section and another 2LE9 in the mechanical one, each consists of 2×1 $(x \times z)$ sub-domains for each. Accordingly, 16LE9 represents 4×2 $(x \times z)$ sub-domains for the mechanical and the piezoelectric cross-sectional domain, respectively. Since special attention will be paid to the detailed stress distribution, the adopted beam models will be further refined until converged stress evaluation is reached.

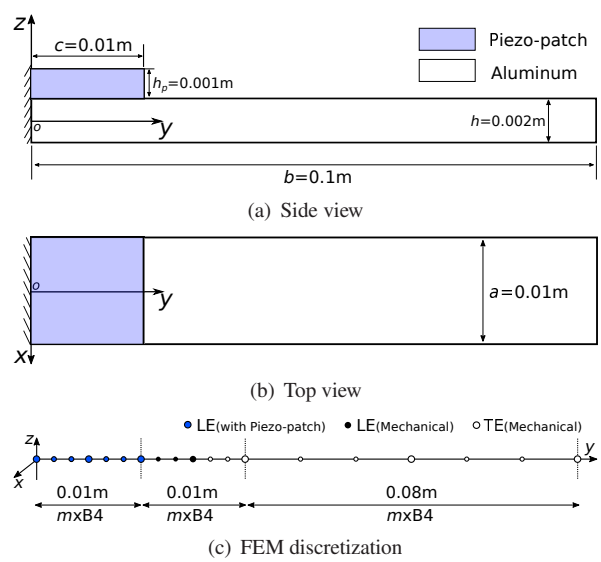

Figure 10. Geometrical feature and FEM discretization of a cantilever beam with a surface-mounted piezo-patch

The refined beam models adopted and their results have been summarised in Table 5, from which the convergence process with the refinement of beam mesh and the nodal kinematics can be observed. It can be found that a FEM model with 24 B4 elements (73 nodes) employing uniform nodal kinematics 16LE9 can guarantee the numerical convergence. Results provided by a three-dimensional ABAQUS model are also listed for comparison. The ABAQUS model consists of piezoelectric brick elements (C3D20RE) with the mesh of $20 \times 20 \times 10$ $(x \times y \times$

Table 4. Material properties of PZT-4

E_1,E_2 [GPa]	E_3 [GPa]	G_{12} [GPa]	G_{13},G_{23} [GPa]	ν_{12}	ν_{13}, ν_{23}	e_{31},e_{32} [C/m^2]	e_{33} [C/m^2]	e_{15},e_{24} [C/m^2]	χ_{11},χ_{22}	χ_{33}
81.3	64.5	30.6	25.6	0.329	0.432	-5.2	15.8	12.72	$1475\chi_0$	$1300\chi_0$

Vacuum permittivity: $\chi_0 = 8.85 \times 10^{-12}$ F/m

z) for the piezo-patch, and another $20 \times 200 \times 10$ brick quadratic elements with reduced integration (C3D20R) for the substrate beam. Biscani et al. (2012) studied this structure with CUF-based plate model employing Lagrange polynomials to the 3rd order through the thickness. CUF-based refined models lead to results in high agreement with the ABAQUS solution as well as that given in Biscani et al. (2012). From Table 5 it can also be observed that the refined beam models have comparable accuracy with the three-dimensional model, but with fewer degrees of freedom.

In contrast with the mono-kinematic LE model, models 16LE9$^{\times 25}$-TE2$^{\times 48}$ and 16LE9$^{\times 49}$-TE2$^{\times 24}$ are constructed according to the scheme illustrated in Figure 10 (c). Here the superscripts indicate the number of nodes on which the corresponding nodal kinematics are adopted. Such models with variable LW/ESL kinematics can reduce the total degrees of freedom. 16LE9$^{\times 49}$-TE2$^{\times 24}$ can lead to results with the same accuracy level but few computational costs comparatively. Meanwhile, model 16LE9$^{\times 49}$-TE2$^{\times 24}$ is more computationally economic but gives less accurate results.

The variations of deflection w and σ_{yy} along the axial direction is as plotted in Figure 11. For deflection w, both 16LE9$^{\times 25}$-TE2$^{\times 48}$ and 16LE9$^{\times 49}$-TE2$^{\times 24}$ lead to continuous and smooth variation along the y axis. Whereas when y goes beyond the range of the zone with refined nodal kinematics, the solution provided by 16LE9$^{\times 25}$-TE2$^{\times 48}$ is comparatively inaccurate. For σ_{yy} distribution along the axis, when the number of nodes employing LE kinematics on the clamped end increases from 25 to 49, a more smooth variation can be achieved and comparable accuracy with the uniform 16LE9 model can be reached.

The contour plot of σ_{yz} on the cross-section $y = c/2$ obtained with the mono-model 16LE9 is as shown in Figure 12, and its changes over the thickness on the edge $(a/2, c/2, z)$ as well as $(x, c/2, 0)$ are as illustrated in Figure 13. The comparison with ABAQUS solution demonstrates that the adopted refined beam model 16LE9$^{\times 49}$-TE2$^{\times 24}$ can provide results with satisfactory accuracy. For 16LE9$^{\times 25}$-TE2$^{\times 48}$, even if refined models are adopted in the patched range, a poor stress estimation in this region is still found because of the unfavourable approximation in the transition region between the peripheral zone and the patched axial range.

Conclusions

Based on Carrera Unified Formulation (CUF), node-dependent kinematic one-dimensional FEM models are proposed for the analysis of structures with embedded and surface-mounted piezo-patches. In the proposed approach advanced beam models with variable LW/ESL nodal kinematics can be formulated. Mechanical and electromechanical constitutive relations are separately applied to the base structure and the piezoelectric actuators. Numerical assessments are conducted through the static analysis of slender cantilever structures with piezo-patches, and both extension and shear mechanisms are considered. The following conclusions can be drawn:

- By applying CUF-based node-dependent kinematics, patches either embedded or attached to the base structure can be modelled with one-dimensional FEM models in a unified manner.
- In the proposed one-dimensional models, the coupled electromechanical constitutive relations are only employed in the domain of the piezo-patches, while pure elastic constitutive relations are applied to the base structure, which is realised with the help of LW models adopting Lagrange expansions.

Table 5. Displacement and stress evaluation on the cantilever beam with a surface-mounted piezo-patch

Mesh	Kinematics	$-u_z[10^{-8}\text{m}]$ $(0,\frac{b}{2},0)$	$-u_z[10^{-8}\text{m}]$ $(0,b,0)$	$-\sigma_{yy}$[KPa] $(0,\frac{c}{2},-\frac{h}{2})$	$-\sigma_{yz}$[KPa] $(\frac{a}{2},\frac{c}{2},0)$	DOFs
12×B4	4LE9	2.482	5.192	5.878	0.5149	2250
12×B4	16LE9	2.444	5.109	5.131	0.6692	12852
24×B4	16LE9	2.452	5.125	5.009	0.6612	25164
24×B4	$16LE9^{\times 25}$-$TE2^{\times 48}$	2.656	5.592	5.028	0.2979	14346
24×B4	$16LE9^{\times 49}$-$TE2^{\times 24}$	2.452	5.125	5.009	0.6612	19908
ABAQUS		2.451	5.125	5.087	0.6381	196281
Biscani-2D(LD3)		2.309	4.871	–	–	–

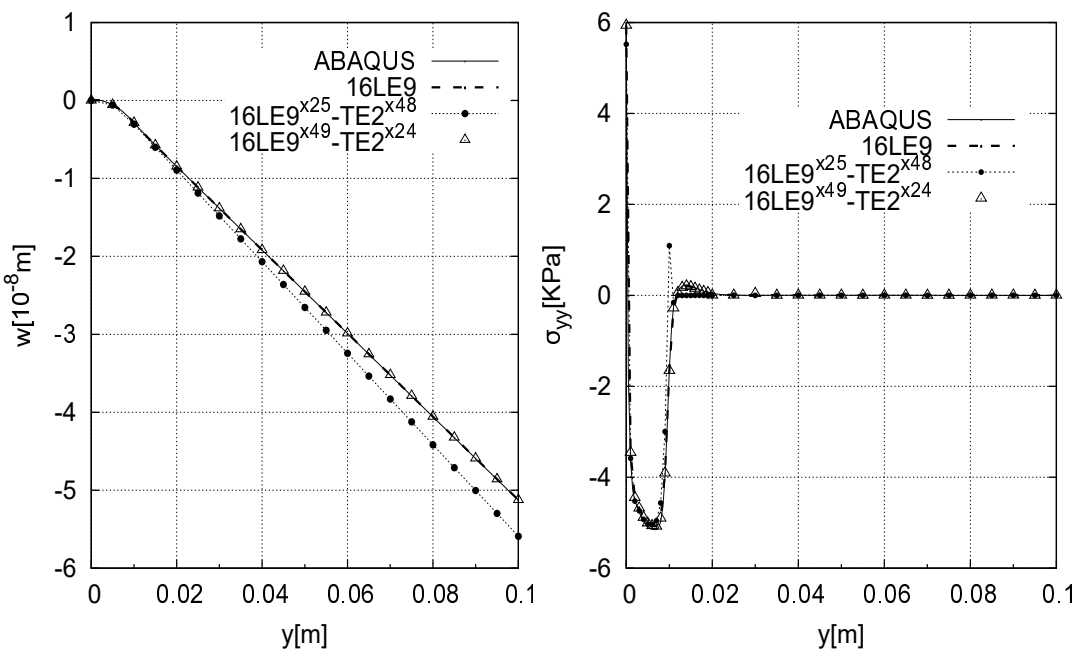

(a) w, $(0,y,0)$ (b) σ_{yy}, $(0,y,-\frac{h}{2})$

Figure 11. Variation of w and σ_{yy} along the axis of the beam with a surface-mounted piezo-patch

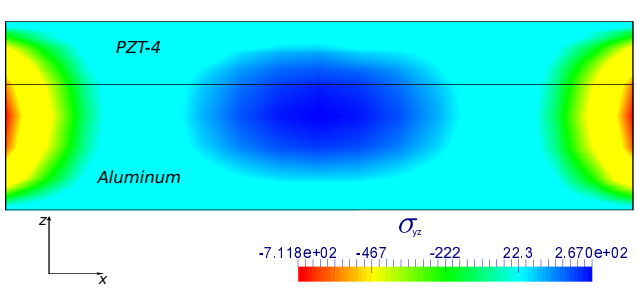

Figure 12. Contour plot of σ_{yz} on cross-section $y = c/2$ of the beam with a surface-mounted piezo-patch, obtained with model 16LE9

- With refined beams models adopting Lagrange expansions, in a unified manner, both extension and shear actuation mechanisms can be appropriately captured.
- Node-dependent kinematic FEM models with variable LW/ESL capabilities can be applied to reduce the computational costs while properly approximating the bending effects of structures under extension actuation.
- Considering the inherent drawback of Taylor series in capturing the transverse shear effects, refined beam

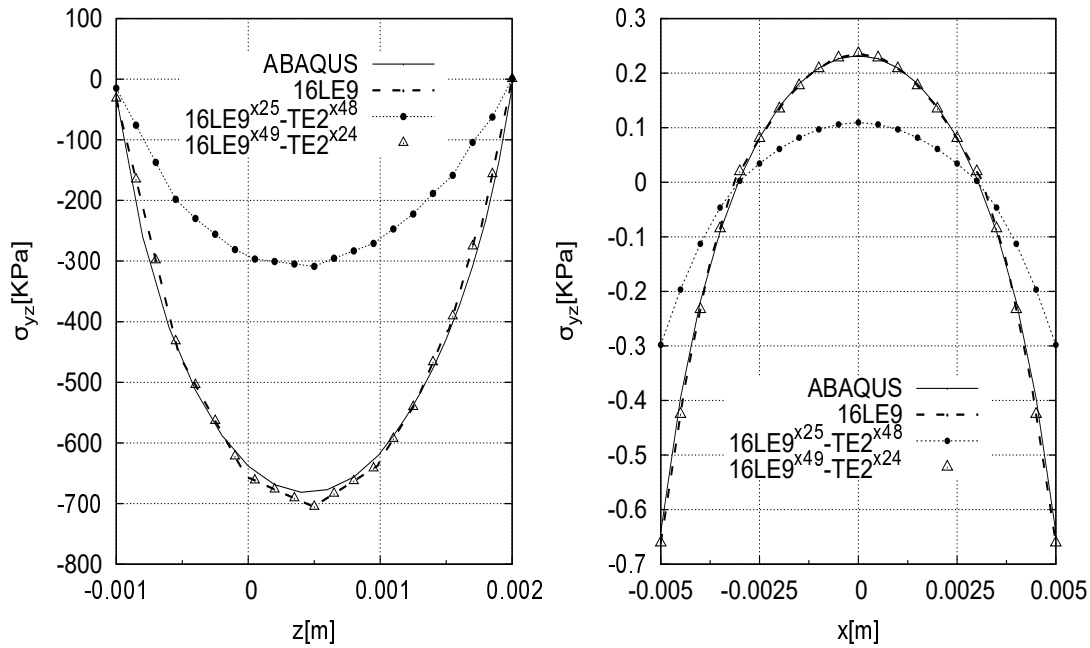

(a) σ_{yz}, $(\frac{a}{2}, \frac{c}{2}, z)$ (b) σ_{yz}, $(x, \frac{c}{2}, 0)$

Figure 13. Variation of σ_{yz} on cross-section $y = c/2$ of the beam with a surface-mounted piezo-patch

models completely discretized with Lagrange-type expansions are preferred to capture the response of structures imposed to shear actuation.

As a versatile approach, CUF-based node-dependent kinematics can be applied to construct numerically efficient one-dimensional FEM models for the analysis of structures with segmented piezoelectric components.

Acknowledgements

This research work has been carried out within the project FULLCOMP (FULLy analysis, design, manufacturing, and health monitoring of COMPosite structures), funded by the European Union Horizon 2020 Research and Innovation program under the Marie Skłodowska Curie grant agreement No. 642121. E. Carrera has been partially supported by the Russian Science Foundation (Grant No. 15-19-30002).

References

Batra R (1995) Deflection control during dynamic deformations of a rectangular plate using piezoceramic elements. *AIAA Journal* 33(8): 1547–1548.

Batra R and Liang X (1997) Finite dynamic deformations of smart structures. *Computational mechanics* 20(5): 427–438.

Beheshti-Aval S, Lezgy-Nazargah M, Vidal P and Polit O (2011) A refined sinus finite element model for the analysis of piezoelectric laminated beams. *Journal of Intelligent Material Systems and Structures* : 1045389X10396955.

Benjeddou A (2000) Advances in piezoelectric finite element modeling of adaptive structural elements: a survey. *Computers & Structures* 76(1): 347–363.

Benjeddou A, Trindade M and Ohayon R (1997) A unified beam finite element model for extension and shear piezoelectric actuation mechanisms. *Journal of Intelligent Material Systems and Structures* 8(12): 1012–1025.

Biscani F, Giunta G, Belouettar S, Carrera E and Hu H (2011) Variable kinematic beam elements coupled via arlequin method. *Composite Structures* 93(2): 697 – 708. DOI: http://dx.doi.org/10.1016/j.compstruct.2010.08.009.

Biscani F, Nali P, Belouettar S and Carrera E (2012) Coupling of hierarchical piezoelectric plate finite elements via Arlequin method. *Journal of Intelligent Material Systems and Structures* 23(7): 749–764.

Carrera E (1996) C0 reissner-mindlin multilayered plate elements including zig-zag and interlaminar stress continuity. *International Journal for Numerical Methods in Engineering* 39(11): 1797–1820.

Carrera E (2002) Theories and finite elements for multilayered, anisotropic, composite plates and shells. *Archives of Computational Methods in Engineering* 9(2): 87–140.

Carrera E, Brischetto S and Nali P (2011a) *Plates and shells for smart structures: classical and advanced theories for modeling and analysis*, volume 36. John Wiley & Sons.

Carrera E, Büttner A and Nali P (2010) Mixed elements for the analysis of anisotropic multilayered piezoelectric plates. *Journal of Intelligent Material Systems and Structures* 21(7): 701–717.

Carrera E, Cinefra M and Li G (2017) Refined finite element solutions for anisotropic laminated plates. *Composite Structures* In press.

Carrera E, Cinefra M, Li G and Kulikov G (2016) MITC9 shell finite elements with miscellaneous through-the-thickness functions for the analysis of laminated structures. *Composite Structures* 154: 360–373.

Carrera E, Cinefra M, Petrolo M and Zappino E (2014) *Finite element analysis of structures through Unified Formulation*. John Wiley & Sons.

Carrera E and Fagiano C (2007) Mixed piezoelectric plate elements with continuous transverse electric displacements. *Journal of Mechanics of Materials and Structures* 2(3): 421–438.

Carrera E, Filippi M and Zappino E (2013) Laminated beam analysis by polynomial, trigonometric, exponential and zig-zag theories. *European Journal of Mechanics-A/Solids* 41: 58–69.

Carrera E, Giunta G and Petrolo M (2011b) *Beam structures: Classical and advanced theories*. John Wiley & Sons.

Carrera E and Robaldo A (2010) Hierarchic finite elements based on a unified formulation for the static analysis of shear actuated multilayered piezoelectric plates. *Multidiscipline Modeling in Materials and Structures* 6(1): 45–77.

Carrera E and Zappino E (2014) Analysis of complex structures coupling variable kinematics one-dimensional models. In: *ASME 2014 International Mechanical Engineering Congress and Exposition*. American Society of Mechanical Engineers, pp. V001T01A023–V001T01A023.

Carrera E and Zappino E (2017) One-dimensional finite element formulation with node-dependent kinematics. *Computers & Structures* In press.

Chandrashekhara K and Agarwal A (1993) Active vibration control of laminated composite plates using piezoelectric devices: a finite element approach. *Journal of Intelligent Material Systems and Structures* 4(4): 496–508.

Cinefra M, Lamberti A, Zenkour AM and Carrera E (2015a) Axiomatic/asymptotic technique applied to refined theories for piezoelectric plates. *Mechanics of Advanced Materials and Structures* 22(1-2): 107–124.

Cinefra M and Valvano S (2016) A variable kinematic doubly-curved MITC9 shell element for the analysis of laminated composites. *Mechanics of Advanced Materials and Structures* 23(11): 1312–1325.

Cinefra M, Valvano S and Carrera E (2015b) Heat conduction and thermal stress analysis of laminated composites by a variable kinematic MITC9 shell element. *Curved and Layered Structures* 2(1).

Crawley EF and Anderson EH (1990) Detailed models of piezoceramic actuation of beams. *Journal of Intelligent Material Systems and Structures* 1(1): 4–25.

Crawley EF and De Luis J (1987) Use of piezoelectric actuators as elements of intelligent structures. *AIAA Journal* 25(10): 1373–1385.

Hauch RM (1995) Industrial approach to static and dynamic finite element modeling of composite structures with embedded actuators. In: *Smart Structures & Materials' 95*. International Society for Optics and Photonics, pp. 458–469.

Heyliger P, Ramirez G and Saravanos D (1994) Coupled discrete-layer finite elements for laminated piezoelectric platess. *International Journal for Numerical Methods in Biomedical Engineering* 10(12): 971–981.

Huang JH and Wu TL (1996) Analysis of hybrid multilayered piezoelectric plates. *International Journal of Engineering Science* 34(2): 171–181.

Jonnalagadda K, Blandford G and Tauchert T (1994) Piezothermoelastic composite plate analysis using first-order shear deformation theory. *Computers & Structures* 51(1): 79–89.

Kapuria S (2001) An efficient coupled theory for multilayered beams with embedded piezoelectric sensory and active layers.

International Journal of Solids and Structures 38(50): 9179–9199.

Kapuria S (2004) A coupled zig-zag third-order theory for piezoelectric hybrid cross-ply plates. *Transactions, American Society of Mechanical Engineers* 71(5): 604–614.

Kapuria S and Hagedorn P (2007) Unified efficient layerwise theory for smart beams with segmented extension/shear mode, piezoelectric actuators and sensors. *Journal of Mechanics of Materials and Structures* 2(7): 1267–1298.

Kapuria S, Kumari P and Nath J (2010) Efficient modeling of smart piezoelectric composite laminates: a review. *Acta Mechanica* 214(1-2): 31–48.

Koutsawa Y, Giunta G and Belouettar S (2013) Hierarchical fem modelling of piezo-electric beam structures. *Composite Structures* 95: 705 – 718. DOI:http://dx.doi.org/10.1016/j.compstruct.2012.08.008.

Koutsawa Y, Giunta G, Nasser H and Belouettar S (2015) Static Analysis of Shear Actuated Piezo-Electric Beams via Hierarchical FEM Theories. *Mechanics of Advanced Materials and Structures* 22(1-2): 3–18. DOI:10.1080/15376494.2014.907946.

Kpeky F, Abed-Meraim F, Boudaoud H and Daya EM (2017) Linear and quadratic solid–shell finite elements shb8pse and shb20e for the modeling of piezoelectric sandwich structures. *Mechanics of Advanced Materials and Structures* : 1–20.

Lee C (1990) Theory of laminated piezoelectric plates for the design of distributed sensors/actuators. Part I: Governing equations and reciprocal relationships. *The Journal of the Acoustical Society of America* 87(3): 1144–1158.

Mackerle J (2003) Smart materials and structuresa finite element approachan addendum: a bibliography (1997–2002). *Modelling and Simulation in Materials Science and Engineering* 11(5): 707.

Miglioretti F, Carrera E and Petrolo M (2014) Variable kinematic beam elements for electro-mechanical analysis. *Smart Structures and Systems* 13(4): 517–546.

Mitchell J and Reddy J (1995) A refined hybrid plate theory for composite laminates with piezoelectric laminae. *International Journal of Solids and Structures* 32(16): 2345–2367.

Robbins D and Reddy J (1991) Analysis of piezoelectrically actuated beams using a layer-wise displacement theory. *Computers & Structures* 41(2): 265–279.

Rogacheva NN (1994) *The theory of piezoelectric shells and plates*. CRC press.

Saravanos DA and Heyliger PR (1999) Mechanics and computational models for laminated piezoelectric beams, plates, and shells. *Applied Mechanics Reviews* 52: 305–320.

Suleman A and Venkayya V (1995) A simple finite element formulation for a laminated composite plate with piezoelectric layers. *Journal of Intelligent Material Systems and Structures* 6(6): 776–782.

Sun C and Zhang X (1995) Use of thickness-shear mode in adaptive sandwich structures. *Smart Materials and Structures* 4(3): 202.

Tiersten HF (1969) *Linear piezoelectric plate vibrations*. Plenum Press, New York.

Tzou H and Gadre M (1989) Theoretical analysis of a multi-layered thin shell coupled with piezoelectric shell actuators for distributed vibration controls. *Journal of Sound and Vibration* 132(3): 433–450.

Vidoli S and Batra R (2000) Derivation of plate and rod equations for a piezoelectric body from a mixed three-dimensional variational principle. In: *Advances in Continuum Mechanics and Thermodynamics of Material Behavior*. Springer, pp. 23–50.

Wang BT and Rogers CA (1991) Laminate plate theory for spatially distributed induced strain actuators. *Journal of Composite Materials* 25(4): 433–452.

Wang J and Yang J (2000) Higher-order theories of piezoelectric plates and applications. *Applied Mechanics Reviews* 53(4): 87–99.

Zappino E, Carrera E, Rowe S, Mangeot C and Marques H (2016) Numerical analyses of piezoceramic actuators for high temperature applications. *Composite Structures* 151: 36–46.

Zappino E, Li G, Pagani A and Carrera E (2017) Global-local analysis of laminated plates by node-dependent kinematic finite elements with variable esl/lw capabilities. *Composite Structures* 172: 1–14.

Zhang X and Sun C (1996) Formulation of an adaptive sandwich beam. *Smart Materials and Structures* 5(6): 814.